physica status solidi

pss

www.pss-journals.com

reprint

WILEY-VCH

Phys. Status Solidi B **248**, No. 4, 892–896 (2011) / **DOI** 10.1002/pssb.201000853

physica status solidi b
www.pss-b.com
basic solid state physics

Progress in growth, fabrication, and characterization of semiconductor photonic crystal nanocavities

B. C. Richards*[,1], J. Hendrickson[1], J. D. Olitzky[1], R. Gibson[1], M. Gehl[1], K. Kieu[1], P. Polynkin[1], G. Khitrova[1], H. M. Gibbs[1], U. K. Khankhoje[2], A. Homyk[2], A. Scherer[2], J.-Y. Kim[3], and Y.-H. Lee[3]

[1] College of Optical Sciences, University of Arizona, 1630 E. University Blvd., Tucson, AZ 85705, USA
[2] Electrical Engineering, California Institute of Technology, 1200 E. California Blvd., Pasadena, CA 91125, USA
[3] Department of Physics, Korea Advanced Institute of Science and Technology, 373-1 Guseong-dong, Yuseong-gu, Daejeon 305-701, Republic of Korea

Received 14 August 2010, accepted 18 September 2010
Published online 24 December 2010

Keywords microcavities, nanophotonics, photonic crystals

* Corresponding author: e-mail brichards@optics.arizona.edu, Phone: +01 520 621 9606, Fax: +01 520 621 4358

We present the results of recent investigations into the fabrication and characterization of high-Q, small mode volume one-dimensional photonic crystal nanobeam cavities in Si and two-dimensional photonic crystal slab nanocavities in GaAs. The nanobeam cavity modes are investigated in transmission by means of a microfiber taper loop apparatus. The spectral transmission profile of the cavity modes is investigated as a function of input polarization into the fiber. The Q of the cavity for different positions and orientations of the fiber taper is investigated. The results are compared to measurements by resonant scattering. The slab nanocavities are investigated by means of quantum dot photoluminescence excitation spectroscopy. We present recent progress in growth and fabrication of such slab nanocavities.

1 Introduction Cavity QED experiments in semiconductors require high quality-factor (Q) and low mode volume nanocavities for confining the electromagnetic field. Photonic crystals have emerged in recent years as a popular system for investigating fundamental light–matter interactions in the QED regime, and have been employed in the observation of several fundamental quantum optics results [1–3]. An important figure of merit for such cavity systems is the ratio Q/V, where V is the effective mode volume of the cavity. Higher values of Q lead to longer photon lifetimes in the cavity (improved chance of light–matter interaction), and smaller values of V lead to higher field intensities (stronger light–matter interaction). The importance of the ratio Q/V can be seen in the expression for Purcell enhancement ($F_p \propto Q/V$) of spontaneous emission and for vacuum Rabi splitting (VRS $\propto Q/\sqrt{V}$) [1, 2, 5–7]. The pursuit of high Q, small V nanocavities has thus been a major focus of efforts in the semiconductor cavity QED community.

Several experimental techniques have been developed and utilized for the purpose of measuring the Qs of photonic crystal nanocavities. The most common technique consists of photoluminescence spectroscopy when the cavity contains active emitters such as quantum dots. This technique usually requires liquid helium temperatures, and also suffers from broadening (narrowing) of the cavity linewidths at low (high) powers due to absorption (gain) by the quantum dots [4]. Two more recent techniques have been developed specifically for the investigation of semiconductor cavity QED systems: a cross-polarized resonant scattering method [8, 9] and a tapered optical microfiber [10, 11]. These two techniques allow the measurement of empty cavity Qs, and hence can be performed at room temperature and without active emitters.

We report the results of our investigations of 1D photonic crystal nanobeam cavities by means of the fiber taper method, and compare the results to those obtained by the resonant scattering method. We observe that the cavity Qs depend on polarization of the light in the fiber, of contact position on the nanobeam, and of angle between the nanobeam and the fiber [12]. We also present recent progress in the growth and fabrication of 2D photonic crystal slab nanocavities in GaAs with InAs QDs [6, 7].

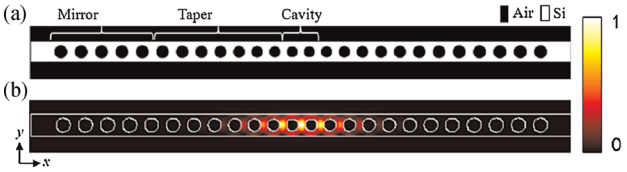

Figure 1 (online color at: www.pss-b.com) (a) Top view of cavity design. (b) Normalized computed electric field profile showing cavity region.

2 Design and fabrication

2.1 Design The first cavity investigated in this study is a photonic crystal nanobeam cavity, which is essentially a wavelength-scale Fabry–Perot etalon formed by sandwiching a 1D photonic crystal waveguide between 1D photonic crystal Bloch mirrors, as shown in Fig. 1. In the transverse directions, the light is confined in the nanobeam by total internal reflection. By smoothly tapering the air hole radius and the corresponding lattice constants in the mirror sections, the scattering loss is minimized and a high Q is achieved [13–15]. 3D finite-difference time-domain (FDTD) simulations [16] reveal that the cavity exhibits a reasonably high Q in excess of 500 000 with very low mode volumes, even though it is placed on a low index substrate. The region of tapered holes in the center of the nanobeam effectively confines the light, analogous to a Fabry–Perot spacer.

2.2 Fabrication The nanobeams are fabricated using electronics grade silicon-on-insulator with a 220 nm silicon device layer and 2 μm buried oxide. To prepare the samples for electron-beam lithography, the wafers are manually cleaved, cleaned with acetone and isopropanol, and the native oxide is removed by a short dip in 10:1 buffered hydrofluoric acid. The samples are then baked at 180 °C, spin-coated with 2% PMMA 950 K in chlorobenzene, and baked again at 180 °C for 5 min. Electron-beam lithography is performed in a Leica EBPG 5000+ at 100 kV. Following electron-beam exposure, the samples are developed in 1:3 MIBK/IPA for 60 s, rinsed in IPA, and dried with nitrogen. After development, the wafers are etched using an Oxford Instruments Plasmalab System100 ICP380 with a mixed-mode gas chemistry consisting of SF_6 and C_4F_8. Figure 2 shows an SEM of one of our nanobeam cavities.

3 Fiber taper loop apparatus

Our nanobeams were investigated by means of a transmission measurement through a tapered microfiber loop that was brought into physical contact with the nanobeam. The tapered region of the fiber is 1–1.5 μm in diameter, and the taper loop has a radius of curvature of 200 μm. The taper loop is produced in two stages, first by heating and pulling a standard single mode optical fiber into a taper, and then by forming the tapered region into a loop in a specially built curving apparatus. The fiber is then glued to a microscope slide in such a way that the loop extends beyond the edge of the slide, and the motion of this assembly is controlled by means of a computer controlled, motorized *xyz* stage.

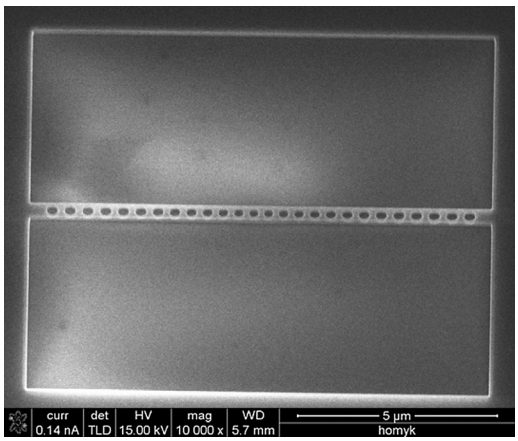

Figure 2 SEM of typical nanobeam cavity.

A beam from an Agilent 8164A mainframe with an Agilent 81682A tunable laser with 0.2 nm wavelength resolution propagates through the fiber and is detected at the output end by means of an InGaAs photodiode. An in-line polarization controller is installed between the laser and the tapered region. The wavelength of the laser is swept across a region of interest, and the output is recorded by a computer. When the tapered loop is moved into physical contact with a nanobeam, light that is propagating through the fiber can be coupled into the mode of the nanocavity, and the resulting interaction is observed as a change in the transmission spectrum output. The laser for this measurement must have a linewidth smaller than the FWHM of a cavity mode, and it must have amplitude fluctuations which are slow compared to the time necessary to scan across a mode. The Q is given by the wavelength of the cavity mode divided by the FWHM of the cavity mode. Figure 3a shows a schematic of the

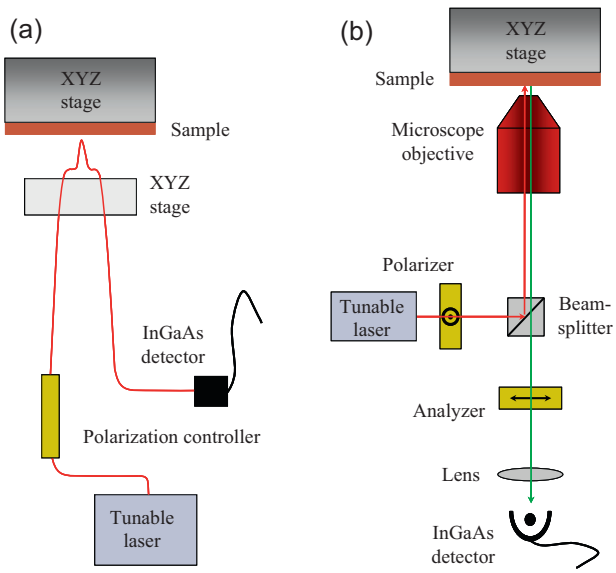

Figure 3 (online color at: www.pss-b.com) (a) Experimental setup for fiber taper loop measurement. (b) Experimental setup for resonant scattering measurement.

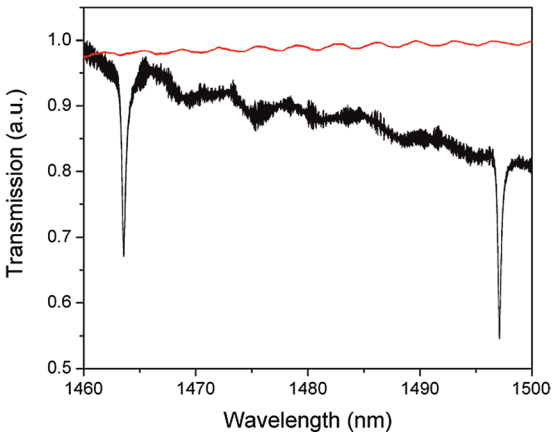

Figure 4 (online color at: www.pss-b.com) Fiber loop transmission spectrum of typical nanobeam cavity at 45°, center contact (black), and spectrum directly from laser (red).

apparatus. Figure 4 shows a typical transmission spectrum of a nanobeam taken with the fiber taper loop apparatus.

4 Coupling to a nanobeam

4.1 Polarization The nanobeams are designed to support a mode which is linearly polarized in a direction perpendicular to the axis of the nanobeam. In order to effectively couple into the cavity mode, the field in the fiber must have a polarization component parallel to the mode of the cavity. Our in-line polarization controller allows us to tune the polarization of the field, and hence control the coupling into the cavity. There are several pathways that the field can travel, each dependent upon the polarization: it can be coupled into the substrate, or it can be scattered back into the fiber in either the forward or the backward direction. As a result of these multiple pathways, we expect to observe interference effects which depend upon the polarization of the incident field, and hence the strength of the coupling into the available channels. We did observe such interference effects, which caused the lineshape of the cavity mode transmission to vary as a function of input polarization, resulting in asymmetric lineshapes. However, by tuning the polarization we were always able to achieve a symmetric lineshape of the transmitted signal.

4.2 Contact pressure The fiber taper loop is brought into contact with the nanobeam, and the motion of the loop is controlled by a motorized *xyz* stage. As the loop comes near to the surface of the sample, electrostatic and Van der Waals forces pull the fiber into the sample, causing it to stick to the nanobeam.

Once the taper loop is in contact with the nanobeam, it can still be advanced or retracted by the actuators, allowing us to adjust the pressure with which the fiber loop contacts the nanobeam. Increased pressure increases the contact length between the fiber taper and the nanobeam, and hence affects the coupling between them, and decreased pressure caused by pulling the taper away likewise decreases the contact length. At some point as the loop is pulled away it pops off the surface of the nanobeam.

Because the contact between the nanocavity and the fiber taper introduces another loss mechanism for light to escape from the cavity, we expect the strength of coupling between the two to affect the measured Q of the cavity. Specifically, if the coupling between the two systems is very strong, we expect to observe lower Qs, and hence the optimal configuration for observing the highest Qs will be the configuration that minimizes the coupling between the fiber taper and the nanobeam, while still allowing enough interaction to observe a change in transmission through the fiber. This expectation was confirmed by our observation of the pressure and contact length affecting the measured Qs of our cavities. To measure the highest Q, it is important to minimize the contact length between the nanobeam and the fiber taper.

4.3 Contact position As seen in Fig. 1, the field profile of the cavity mode is concentrated near the center of the nanobeam. As a result, we expect the coupling between the fiber loop and the nanobeam to depend on the position along the length of the nanobeam at which contact is made: contact at the center should result in the strongest coupling, and contact at the edge should result in the weakest coupling. We confirmed that this is in fact the case, and that to measure the highest Qs, the taper loop should be brought into contact as close to the edge of the nanobeam as will still produce a modification in the transmission. Contact near the center of the nanobeam also produces a modification of the refractive index in the environment of the cavity mode, resulting in a shift of the wavelength of the observed resonance.

4.4 Contact angle Because the polarization of the cavity mode is always linearly polarized in the same direction, the coupling between the fiber taper and the cavity mode can also be varied by changing the angle between the fiber taper loop and the axis of the nanobeam. The sample itself is mounted on a rotary stage that allows us to rotate the sample about an axis normal to the sample surface. Whereas the polarization controller only allows control over the polarization along the axis of the fiber, rotating the sample with respect to the fiber provides another degree of control over the coupling.

When the fiber is oriented parallel to the nanobeam, we expect that the field polarization can always be tuned such that it has a component parallel to the mode of the cavity where the coupling between them will be the strongest. Alternatively, when the fiber taper is contacted in a configuration perpendicular with respect to the nanobeam, we would expect that the field never has a component parallel to the cavity mode, and hence coupling between the two will be minimal.

We found that in the parallel configuration, the coupling was indeed the strongest, and the Q the lowest. As we tuned the angle between the nanobeam and the fiber away from parallel, the Q improved, but at angles close to the

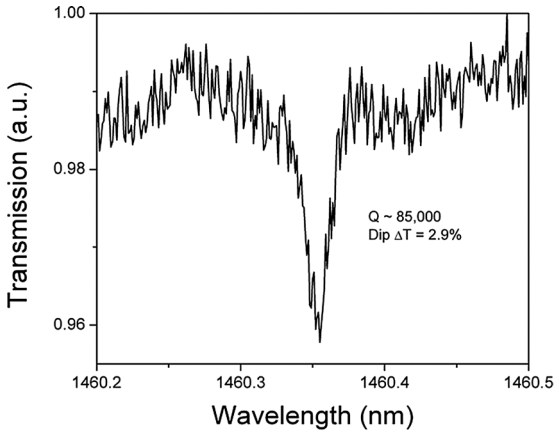

Figure 5 Fiber loop transmission spectrum of high-Q cavity mode, at 45°, edge contact, with $Q = 85\,000$.

perpendicular configuration, there was not enough coupling to observe a change in the transmitted signal.

4.5 Results The highest Qs were observed with an angle of the fiber taper between 20 and 60° with respect to the nanobeam axis, and contact made at the edge of the nanobeam. This configuration minimizes the contact between the loop and the nanobeam, but still supports a polarization component corresponding to the cavity mode. The highest Q measured in our system was 85 000, which with a computed mode volume of $0.27(\lambda/n)^3$, yields Q/V of 315 000, which we believe to be the highest Q/V reported in nanobeams on substrate. The group of De La Rue [17] reported a Q of 147 000 with a computed mode volume of $0.85(\lambda/n)^3$, yielding Q/V of 173 000. Figure 5 shows the transmission spectrum of our highest Q cavity mode.

5 Comparison to resonant scattering Another method commonly used for measuring the Qs of semiconductor nanobeam cavities is a cross-polarized resonant scattering technique [8, 9], shown in Fig. 3b. Whereas the fiber taper measurement introduces an additional loss mechanism to the cavity, and hence lowers the Q, the resonant scattering technique does not affect the Q of the cavity, and hence provides a more accurate measurement of the intrinsic Q. We compared the two techniques and found that the Qs measured by resonant scattering were higher than those measured on the same cavity by fiber taper loop. However, the resonant scattering technique also suffers from some drawbacks. First, in the spectral region of our cavity modes and within the range of our tunable laser, 1460–1580 nm, there is a number of absorption lines due to atmospheric nitrogen, which also appear as dips in the detected signal similar to the cavity modes of the nanobeams. If one of these lines is spectrally coincident with the mode of a cavity, it is not possible to distinguish the dip of the cavity mode from the dip due to nitrogen absorption. This was unfortunately the case with our highest Q cavity of 85 000 that was measured with the fiber taper. In order to overcome this difficulty, the cavity mode would have to be tuned away from the nitrogen resonance, for instance by heating or by condensation of xenon or nitrogen gas [18]. Second, the resonant scattering method is known to exhibit asymmetric lineshapes. This is attributed to a Fano interference between the resonantly scattered light and the coherent background, and requires that a Fano lineshape be fit to the data in order to determine the cavity Q. Galli et al. have reported [19] that the asymmetry of the lineshape can be changed by changing the spot size of the incident laser beam.

In addition to these considerations, the two methods also differ in ease of setup and use. The fiber taper loop is very robust and easy to use once it is set up; however, the fabrication of the fiber taper loop itself requires special equipment and experience. The resonant scattering method can be set up with standard optical laboratory components and instruments, but it is extremely sensitive to alignment and hence more difficult to use. Both methods are useful at room temperature as well as at cryogenic temperatures, but the fiber loop measurement would require substantial modification to most cryostats for low temperature measurements. The resonant scattering measurement does not require components inside the cryostat.

6 2D GaAs slab nanocavities While nanocavities in silicon achieve very high Qs, GaAs remains the system of choice for quantum optics experiments because of the ease of incorporating active emitters, such as InAs QDs, which has so far remained elusive for Si. The majority of our research focuses on the GaAs/InAs 2D photonic crystal slab system for the purpose of quantum optics experiments. However, in spite of extensive efforts by the cavity QED community aimed at reaching high Qs at shorter wavelengths in GaAs PC nanocavities, the results have been disappointing compared to what has been achieved at longer wavelengths in GaAs [20] and Si.

In the course of work toward optimizing the growth and fabrication of such GaAs 2D nanocavities, AFM of the sample surface was used extensively for characterizing the quality of the growth. We found, that even on samples where AFM showed a smooth surface, TEM images revealed that the top of the AlGaAs sacrificial layer could be very rough, with the roughness larger along one crystal axis. Changing certain MBE growth parameters reduced the roughness, but this did not result in a noticeable increase in Q [7], indicating that other loss mechanisms are still holding down the Qs. With future improvements in fabrication, we expect the smoothness of the AlGaAs layer to be significant.

Investigations of the sample surfaces by AFM and SEM also revealed debris on the surface of the samples that we believed to be an artifact of the HF acid wet etch. A 140 s dip in a KOH solution removed the debris, confirming that it was most likely a hydroxide of aluminum generated during the wet etch. The measured Qs of the cavities did improve noticeably following the removal of this debris, by an average of 50% on 10 different nanocavities, and the intensity of the photoluminescence also increased [7].

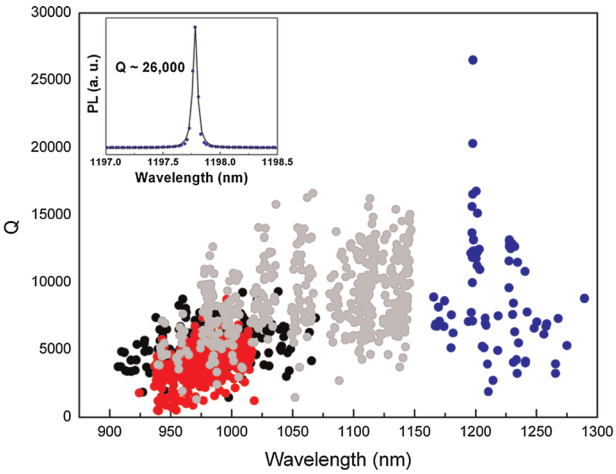

Figure 6 (online color at: www.pss-b.com) Scatter plot of *Q*s from four different samples: QD24-3 (black), QD25-3 (red), A0961-3 (gray), and QD58-1 (blue).

Such improvements in growth and fabrication have yielded modest improvements in the *Q*s we have been able to achieve. Nevertheless, we still consistently observe that even our best samples show lower *Q*s as wavelength decreases. Figure 6 shows *Q* versus wavelength data for several 100 nanocavities from four of our best samples covering a broad wavelength range from 900 to 1300 nm. The data show a decisive decrease in *Q* in the shorter wavelength region. The highest *Q* measured was 26 000, and the PL spectrum for this nanocavity is shown in the inset to Fig. 6.

7 Conclusion We have succeeded in measuring the *Q*s of photonic crystal nanobeam cavities using a fiber taper loop, and have observed *Q*s as high as 85 000, which yields the highest *Q*/*V* ratio reported in these devices on substrate. We have observed that the results of this technique depend on strength of contact between the fiber and the nanobeam, incident field polarization, contact position on the nanobeam, and angle between the fiber loop and the nanobeam. We compared our results to the cross polarized resonant scattering method, and found that the fiber loop does lower the *Q*s, but that the effect can be minimized and high *Q*s can still be measured by choosing the above parameters appropriately.

Acknowledgements The USA authors would like to acknowledge support (EEC-0812072) from the National Science Foundation (NSF) through the Engineering Research Center for Integrated Access Networks (CIAN). The Tucson group also acknowledges support from NSF Atomic Molecular and Optical Physics (AMOP) and Electronics, Photonics, and Device Technologies (EPDT), AFOSR, and Arizona Technology & Research Initiative Funding (TRIF). The Caltech authors gratefully acknowledge critical support and infrastructure provided for this work by the Kavli Nanoscience Institute at Caltech. H. M. G. thanks the Alexander von Humboldt Foundation for a Renewed Research Stay. A. H. appreciates the generous support of the ARCS Foundation.

References

[1] T. Yoshie, A. Scherer, J. Hendrickson, G. Khitrova, H. M. Gibbs, G. Rupper, C. Ell, O. B. Shchekin, and D. G. Deppe, Nature **432**, 200–203 (2004).
[2] D. Englund, D. Fattal, E. Waks, G. Solomon, B. Zhang, T. Nakaoka, Y. Arakawa, Y. Yamamoto, and J. Vuckovic, Phys. Rev. Lett. **95**, 013904 (2005).
[3] D. Press, S. Gotzinger, S. Reitzenstein, C. Hofman, A. Loffler, M. Kamp, A. Forchel, and Y. Yamamoto, Phys. Rev. Lett. **98**, 117402 (2007).
[4] J. Hendrickson, B. C. Richards, J. Sweet, S. Mosor, C. Christenson, D. Lam, G. Khitrova, H. M. Gibbs, T. Yoshie, A. Scherer, O. B. Shchekin, and D. G. Deppe, Phys. Rev. B **72**, 193303 (2005).
[5] G. Khitrova, H. M. Gibbs, M. Kira, S. W. Koch, and A. Scherer, Nature Phys. **2**, 81–90 (2006).
[6] U. K. Khankhoje, S.-H. Kim, B. C. Richards, J. Hendrickson, J. Sweet, J. D. Olitzky, G. Khitrova, H. M. Gibbs, and A. Scherer, Nanotechnology **21**, 065202 (2010).
[7] J. Sweet, B. C. Richards, J. D. Olitzky, J. Hendrickson, G. Khitrova, H. M. Gibbs, D. Litvinov, D. Gerthsen, D. Z. Hu, D. M. Schaadt, M. Wegener, U. Khankhoje, and A. Scherer, Photon. Nanostruct. Fundam. Appl. **8**, 1–6 (2010).
[8] M. W. McCutcheon, G. W. Rieger, I. W. Cheung, J. F. Young, D. Dalacu, S. Frédérick, P. J. Poole, G. C. Aers, and R. L. Williams, Appl. Phys. Lett. **87**, 221110 (2005).
[9] D. Englund, A. Faraon, I. Fushman, N. Stoltz, P. Petroff, and J. Vučković, Nature **450**, 857–861 (2007).
[10] K. Srinivasan, P. E. Barclay, M. Borselli, and O. Painter, Phys. Rev. B **70**, 081306(R). (2004).
[11] I.-K. Hwang, G.-H. Kim, and Y.-H. Lee, IEEE J. Quantum Electron. **42**, 131–136 (2006).
[12] B. C. Richards, J. Hendrickson, J. D. Olitzky, R. Gibson, M. Gehl, K. Kieu, U. K. Khankhoje, A. Homyk, A. Scherer, J.-Y. Kim, Y.-H. Lee, G. Khitrova, and H. M. Gibbs, Opt. Express **18**, 20558–20564 (2010).
[13] P. Deotare, M. McCutcheon, I. Frank, M. Khan, and M. Loncăr, Appl. Phys. Lett. **94**, 121106 (2009).
[14] C. Sauvan, P. Lalanne, and J. Hugonin, Phys. Rev. B **71**, 1–4 (2005).
[15] E. Kuramochi, H. Taniyama, T. Tanabe, K. Kawasaki, Y.-G. Roh, and M. Notomi, Opt. Express **18**, 15859–15869 (2010).
[16] A. Oskooi, D. Roundy, M. Ibanescu, P. Bermel, J. Joannopoulos, and S. Johnson, Comput. Phys. Commun. **181**, 687702 (2010).
[17] A. R. M. Zain, N. P. Johnson, M. Sorel, and R. M. De La Rue, Opt. Express **16**, 12084–12089 (2008).
[18] S. Mosor, J. Hendrickson, B. C. Richards, J. Sweet, G. Khitrova, H. M. Gibbs, T. Yoshie, A. Scherer, O. B. Shchekin, and D. G. Deppe, Appl. Phys. Lett. **87**, 141105 (2005).
[19] M. Galli, S. L. Portalupi, M. Belotti, L. C. Andreani, L. O'Gaolain, and T. F. Krauss, Appl. Phys. Lett. **94**, 071101 (2009).
[20] S. Combrié, A. De Rossi, Q. V. Tran, and H. Benisty, Appl. Phys. Lett. **87**, 141105 (2005).